



Enhancing the Photocatalytic Degradation of Selected Estrogenic Hormone Using ZnO/Hydroxyapatite Nanocomposite

C. El Bekkali¹ · M. Abbadi^{1,2} · J. Labrag¹ · I. Es-saidi¹ · D. Robert² · J. M. Nunzi³ · A. Laghzizil¹

Received: 19 February 2024 / Accepted: 21 April 2024 / Published online: 8 May 2024
© The Tunisian Chemical Society and Springer Nature Switzerland AG 2024

Abstract

Combining 40wt.% ZnO with HAP within a low-cost coprecipitation method results in a 40ZnO:HAP composite with a high specific surface area of $250 \text{ m}^2\text{g}^{-1}$ that is able to retain the 17α -ethinyl estradiol (EE2), a hormonal model, and then degrade it under UV light. The particle size is between 10 and 20 with platelet morphology of approximately 5 nm. Due to the large structure of EE2, its adsorption on ZnO, HAP and 40ZnHAP is low, but it is easily degraded under UV light. The experimental adsorption kinetics matches well with the pseudo-first-order equation and the maximum adsorption capacity (q_e) is the highest for the 40ZnHAP nanocomposite though it does not exceed 1.1 mg g^{-1} . The complete degradation of EE2 is achieved for 40ZnHAP and ZnO at 90 min and 120 min, respectively. Results indicate that the combination of ZnO and porous apatite is an interesting combination for the efficient degradation of EE2 hormone.

Keywords 17α -ethinylestradiol Hormone · ZnO:HAP Nanocomposite · Adsorption · Photocatalytic Degradation

1 Introduction

Many pharmaceutical residues are hazardous in nature and intrinsically dangerous as well as persistent in the environment because they are poor substrates for indigenous micro-organisms [1, 2]. They have been found worldwide in soil and water. Among them, antibiotics and hormones have been used in large quantities for several decades for human and veterinary medicine and as growth promoters in animal husbandry. The elimination of these toxic species from wastewater is therefore of major importance [3–5].

Recently, several physico-chemical treatments have been proposed for efficient pharmaceutical removal, such

as adsorption [6, 7], wet oxidation [8], ozonation [9], and heterogeneous photocatalysis [10, 11]. The simultaneous adsorption and heterogeneous photocatalysis have attracted special attention for the removal of micro-contaminants in the environment using low-cost raw materials. It is based on the activation of a semiconductor by light of those porous TiO_2 is commonly used, while ZnO is considered an alternative material despite being non-porous [12]. TiO_2 nanoparticles are an efficient photoactive material to reduce environmental pollution through to its high photo-catalytic activity. The catalytic efficiency of pure TiO_2 is limited by a low rate of electron transfer to oxygen and a strong recombination of electron–hole pairs [13]. Association with various metal oxides shifts the activity of TiO_2 towards the visible range and improves its photocatalytic activity [14]. Rare-earth-doped- TiO_2 photocatalyzed 17α -methyltestosterone degradation in aqueous solution, with the best photocatalytic mineralization performance for Sm-doped TiO_2 [15]. Compared with pure ZnO, rare-earth doped ZnO nanocomposite improved the photocatalytic degradation of tetracycline antibiotic under visible light and maintained high stability for catalyst regeneration [16]. Various xenobiotic organic compounds (XOCs) are also eliminated by photocatalytic using ZnO nanoparticles [17]. ZnO particles were tested for the effective piezo-photocatalytic degradation of the emerging contaminants testosterone and β -estradiol in

✉ A. Laghzizil
laghzizi@fsr.ac.ma

¹ Laboratory of Applied Chemistry of Materials, Faculty of Science, Mohammed V University in Rabat, Avenue Ibn Batouta BP.1014, Rabat, Morocco

² Institut de Chimie Et Procédés Pour L'Energie, L'Environnement Et La Santé (ICPEES), CNRS-UMR7515, Université de Strasbourg, Saint-Avold Antenna, Université de Lorraine, 12 Rue Victor Demange, 57500 Saint-Avold, France

³ Department of Physics, Engineering Physics and Astronomy, Queen's University, Kingston, ON, Canada

water [18]. However, ZnO nanoparticles have a strong tendency to aggregate, which limits the photocatalytic degradation. ZnO modification like the association with a porous mineral happens to overcome this issue [19]. Although hydroxyapatite has good retention efficiency for the majority of organic pollutants, it is less effective as a photocatalyst although some empirical and statistical work describes the opposite [20–22]. In this context, the association of ZnO with porous hydroxyapatite (HAP) prepared from Moroccan natural phosphate (ZnHAP) at low cost can prove very effective in degrading certain pharmaceutical residues and trapping by-products resulting from photocatalytic degradation, understanding that these can be even more toxic than the parent drug.

A photocatalytic degradation of emerging antibiotic pollutants in water by TiO₂/HAP [23] and ZnO-HAP [24, 25] nanocomposite materials was achieved where 40TiO₂/HAP and 40ZnO/HAP are efficient catalysts for the enhanced adsorption and photocatalytic degradation of ciprofloxacin and ofloxacin. The relationship between structural, surface properties and chemical composition of nanocomposites with their photodegradation efficiency has been discussed. These nanocomposites were easily regenerated by heat treatment at 500°C without significant loss of catalytic efficiency. Therefore, the 40ZnO-HAP catalyst (called 40ZnHA) is efficient and environmentally friendly to remove various antibiotics from water. The extension to other pharmaceutical residues should make it possible to analyse the effectiveness of the 40ZnHAP nanocomposite to clarify the different reactions involved between the pollutant and its catalyst catalytic surface as well as the underlying mechanisms which occur within it. Hormones are also an important contaminants in water resources, whose effects on health and the environment are now fully considered and estimated [26, 27]. In fact, their release into the environment without pre-treatment disrupts the endocrine systems, causing toxic effects for the aquatic environment [28–30]. This study develops and evaluates the 40ZnHAP nanocomposite prepared from natural phosphate in the presence of Zn²⁺ ions and evaluated its photodegradation efficiency against a steroid hormone 17 α ethinylestradiol (named EE2). Kinetics of adsorption and photocatalytic degradation of EE2 as homonal model using three photocatalysts as ZnO, HAP, and 40ZnHAP composites.

2 Materials and Methods

2.1 Synthesis

The pure hydroxyapatite powder (HAP) was prepared by a dissolution/precipitation method from a natural phosphate coming from the Bengurir region (Morocco) as previously

described elsewhere [31]. ZnO was prepared by precipitation of zinc nitrate dihydrate Zn(NO₃)₂·2H₂O with a solution of ammonia in water (NH₄OH, 25%) which is perfectly compatible with the synthesis conditions of HAP. The 40ZnHAP powder was obtained from the natural phosphate by a dissolution/reprecipitation method in the presence of Zn²⁺ ions as described elsewhere [24].

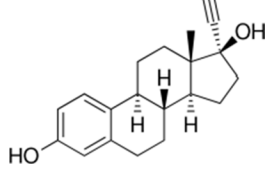
2.2 Techniques

The crystalline phases were identified using a powder X-ray diffractometer (XRD) (Philips PW131 diffractometer) with CuK α source ($\lambda = 1.5406\text{\AA}$) operating at 40kV and 30mA. The N₂ adsorption–desorption isotherms for dried powders were obtained by multi-point N₂-gas sorption experiments at 77 K using a Micromeritics ASAP 2010 instrument. The specific surface areas were calculated according to the Brunauer–Emmett–Teller (BET) method using adsorption data in the relative pressure range from 0.05 to 0.25 whereas the pore size and volume were estimated using the Barret–Joyner–Halenda (BJH) approximation. The sample powder was chemically analyzed by inductively coupled plasma (ICP-AES) emission spectroscopy (ICPS-7500, Shimadzu, Japan). The particle morphologies were determined by SEM/EDX on a JEOL/EO IP100, and TEM on a Tecnai G2 apparatus operating at 100 kV.

2.3 Adsorption and Photocatalytic Degradation Experiments

The adsorption kinetics were followed in batch experiments carried out at 23°C by adding 200 mg of each adsorbent (HAP, ZnO and 40ZnHAP) to 100 mL of water containing 10 mg L⁻¹ of 17 α -ethinylestradiol hormone (EE2); its characteristics are given in Table 1. The pH of the mixture is raised without adjustment (towards 6.5) and the suspension is kept under magnetic stirring. At selected time interval, samples of 5 ml were taken, filtered using a 0.45 μm membrane filter and the EE2 concentration in supernatant was analyzed using a UV–visible spectrophotometer (VWR UV-3100PC) at 365 nm. The amount of adsorbed hormone q_t (mg g⁻¹) was measured by the difference between the initial (C_0) and instantaneous (C_t) concentration of the hormone molecule in the solution according to the equation $q_t = \frac{(C_0 - C_t)}{m} \cdot V$, where m and V are the mass of adsorbent and the volume of solution respectively. The obtained kinetics data were fitted with the linear form of the Lagergren pseudo first-order equation $\log(q_e - q_t) = \log q_{e,1} - \frac{k_1}{2.303} t$, where $q_{e,1}$ (mg g⁻¹) is the amount at equilibrium of adsorbed hormone per gram of sorbent and k_1 is the pseudo-first order rate constant. The linear form of the Lagergren pseudo-second-order equation $\frac{1}{q_t} = \frac{1}{k_2 q_{e,2}^2} + \frac{1}{q_{e,2}} t$, with $q_{e,2}$ (mg g⁻¹), the

Table 1 Physicochemical characteristics of 17 α -ethynylestradiol hormone

Formula	Molar mass (g mol ⁻¹)	Structure	Solubility in water (mg L ⁻¹) at 27°C	pK _a [32]	log K _{ow} [32]
C ₂₀ H ₂₄ O	296.41		4.8-11.3	10.5-	3.6-
2				10.7	4.15

amount at equilibrium of adsorbed molecule per gram of sorbent and k_2 the pseudo-second order rate constant.

For photocatalysis experiments, the photoreactor used is an open-necked Pyrex cylinder with a capacity of 150 mL, giving the possibility of introducing solutes and taking samples. It is equipped with a HPK high pressure mercury vapor dipping lamp (Philips 125 W) and a cooling system through the circulation of water in a double-walled envelope equipped with a stirring system. The photocatalytic activity of three powders ZnO, HAP and 40ZnHAP heated at 500°C was evaluated under UV A-B-C irradiation of 125W (200–600 nm). Each 200 mg sample was initially dispersed in 100 ml EE2 solution (10 mg L⁻¹) and left to react in the dark for 60 min to establish an adsorption/desorption equilibrium on the catalyst surface before UV-irradiation. Then, the solution was exposed to UV light under magnetic stirring. At selected time, the suspensions were centrifuged at 4000 rpm for 20 min, and the supernatants were kept in the dark before analysis.

3 Results and Discussion

3.1 Characterization Overview

The resulting powders of ZnO, HAP and their 40ZnHAP nanocomposite were characterized by XRD technique (Fig. 1). After calcined at 500°C, broad diffraction peaks of the hydroxyapatite structure were well identified for the pure HAP (JCPDS 09–0432) [33] while ZnO sample showed the main diffraction peaks of the zincite structure (JCPDS 36–1451) [34]. These two structures are found in the 40ZnHAP nanocomposite powder calcined at 500°C. No secondary phase such as zinc phosphates was detected.

The textural properties of the prepared samples were investigated by SEM and TEM analyses. Before being analyzed, the powders are deposited on an adhesive carbon membrane. SEM images of ZnO calcined at 500°C show

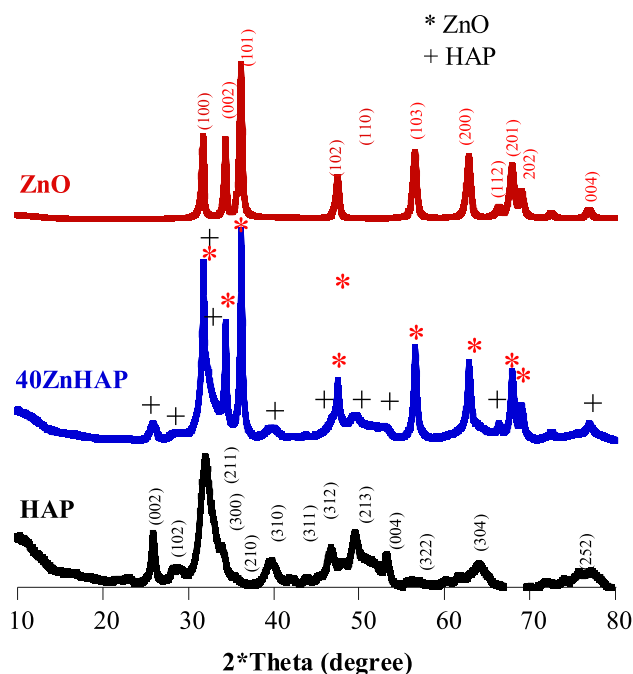


Fig. 1 XRD patterns of photocatalysts calcined at 500°C

only hexagonal aggregates but sometimes fused particles of different morphologies while the HAP and 40ZnHAP particles agglomerate and difficult by SEM analysis to determine the particle size of the materials studied. However, this analysis provides information on the homogeneity of the samples and, more particularly, on the dispersion of the ZnO in porous HAP network. Compared to ZnO and HAP, the EDX analysis confirmed the presence of Ca, P, O and Zn chemical elements in 40ZnHAP powder without taking into consideration the carbon peak from the carbon adhesive membrane.

TEM studies indicate that these powders consist of aggregated nanoparticles (Fig. 2). The pure HAP powder consists of agglomerates with particle sizes between 20–50

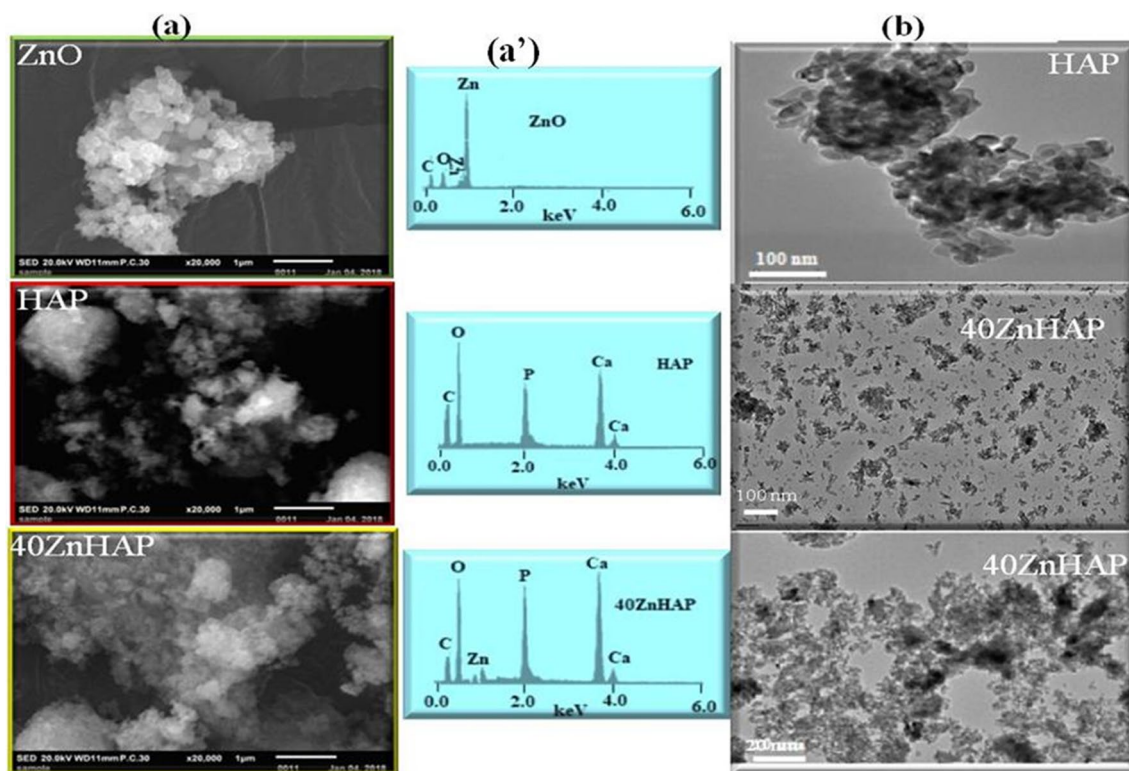


Fig. 2 a, a' SEM/EDX and (b) TEM images of calcined powders

nm, while 40ZnHAP powder consists of visibly separated rod-shaped particles (10–20) with platelet morphologies of about 5 nm. Notably, 40ZnHAP exhibits a rather open structure with easily distinguishable individual particles and the aggregation density seems to increase especially visible at high magnification (scale bar = 20 nm). It should be noted that the association of ZnO with HAP reduces the size of the particles.

ICP-AES analyzes were performed to determine the amounts of Ca, P and Zn in the 40ZnHAP nanocomposite (Table 2). In 40ZnHAP, the experimental and theoretical values of the Zn/Ca molar ratio are the same and close to 0.48, which suggests that there is no loss of Ca^{2+} and Zn^{2+} ions during the preparation of the composite.

The specific surface area of the powders was calculated from N_2 sorption measurements for dried and calcined powders by applying the BET method (Table 2). After drying

at 100°C , the 40ZnHAP nanocomposite has a specific surface area S_{BET} of $250 \text{ m}^2\text{g}^{-1}$, greater than that of pure HAP ($165 \text{ m}^2\text{g}^{-1}$) and much greater than that of ZnO ($20 \text{ m}^2\text{g}^{-1}$) (Table 2). This may be related to the inhibition of grain crystal growth by the addition of Zn^{2+} ions to the HAP precipitation solution which promotes the creation of pores. Average pore size D_p was 11 for 40ZnHAP, slightly larger (14 nm) for HAP and significantly smaller (4 nm) for ZnO. After heat treatment at 500°C , all S_{BET} values have significantly decreased due to crystalline grain growth, but the nanocomposite powder keeps good surface properties than HAP and ZnO.

The optical properties of the prepared powders were determined by diffuse reflection spectroscopy using the Wood-Tauc's equation $(\alpha h\nu)^2$ vs $(h\nu)$ [35] where α is absorption coefficient, E_g is the optical band gap of the material. E_g is identified by extrapolating the linear portion of the

Table 2 Chemical analyses, Specific surface area (S_{BET}) and Average pore size (D_p)

	Ca (wt.%)	P (wt.%)	Zn (wt.%)	Ca/P molar ratio	$S_{\text{BET}100}$ ($\text{m}^2 \text{g}^{-1}$)	D_p100 (nm)	$S_{\text{BET}500}$ ($\text{m}^2 \text{g}^{-1}$)	D_p500 (nm)
HAP	37.90	15.92	-	1.89	165	14	105	12
40ZnHAP	32.15	15.01	25.18	1.65	250	11	135	11
ZnO	-	-	-	-	20	4	10	9

plots of $(\alpha h\nu)^2$ against $(h\nu)$ to the energy axis. The calculated E_g values of ZnO and HAP powders were 3.2 eV and 5.3 eV respectively, while that of 40ZnHAP is around 3.7 eV such as published in our previous work [35]. Therefore, the composite presents an intermediate energy gap between ZnO and HAP.

3.2 Hormone Adsorption

To understand the movement of EE2 into and through the sites on the surface of ZnO, HAP and 40ZnHAP adsorbents, the adsorption kinetics were studied at fixed 10 ppm of EE2 in the dark. Compared to ZnO and HAP powders, 40ZnHAP showed a significant adsorption capacity and the time to reach equilibrium was around 60 min for HAP and 40HAP and 90 min for ZnO (Fig. 3). To further analyze these results, two kinetic models, Lagergren pseudo-first-order and pseudo-second-order equations, were evaluated to fit the experimental data. The best fitting model was selected based on the values of the linear regression correlation coefficient. The correlation coefficients, R^2 , the rate k_i , and sorption capacity, $q_{e,i}$, are gathered in Table 3. The amount of adsorbed EE2 hormone does not exceed about 1.1 mg g⁻¹ for the nanocomposite and it is lower for ZnO and HAP, which requires another process based on heterogeneous photocatalysis.

Compared to the pseudo-second order fit, the first order model fits better the experimental data, especially for HAP, which evidences a physisorption mechanism. This indicates that the adsorption of EE2 on the adsorbents is controlled by external and internal diffusion processes followed by a surface reactivity between the surface functions of the

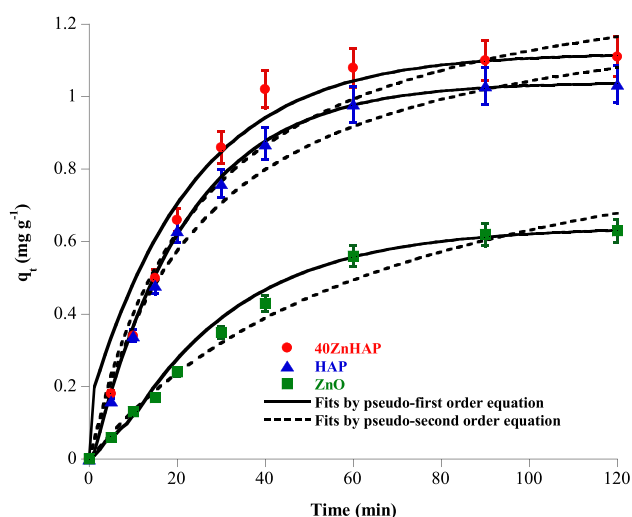


Fig. 3 Adsorption kinetics of 17 α -ethinylestradiol onto different photocatalysts. Error bars represent the standard deviation of triplicate experiments

Table 3 Parameters obtained by simulating the sorption data of the hormone EE2 on HAP, ZnO and the 40ZnHAP nanocomposites according to the two kinetic models proposed

		HAP	40ZnHAP	ZnO
$q_{e,exp}$ (mg g ⁻¹)		1.03	1.11	0.63
Pseudo first order	k_1 (min ⁻¹)	0.051	0.042	0.037
	$q_{e,1}$ (mg g ⁻¹)	1.18	0.97	0.76
	R^2	0.9954	0.9779	0.9944
Pseudo second order	k_2 (min ⁻¹)	0.045	0.034	0.023
	$q_{e,2}$ (g mg ⁻¹ min ⁻¹)	1.19	1.33	0.88
	R^2	0.9908	0.9857	0.9642

adsorbent and the active groups of the hormone. Bulk porous diffusion, surface diffusion or both can influence adsorption kinetics depending on the porosity and composition of the adsorbent. Moreover, this diffusion is also strongly influenced by nanostructuring the adsorbents, with kinetics that depend on the nature of the Van de Waals interactions and the hydrogen bonds between solute/ and adsorbent. This reveals the kinetic differences between the three materials ZnO, HAP and 40ZnHAP composite that are characterized by a variation of porosity and oxygenated species on their surface, of which 40ZnHAP composite combines the best characteristics of the two materials. For this, the kinetic alteration observed shows that the mechanism of adsorption of EE2 on 40ZnHAP differs slightly from that on HAP and ZnO.

Overall, the adsorption process can be rationalized as follows: the hormone is first adsorbed on the surface of the apatite grains where interactions occur between EE2 and the apatite surface being the most porous and containing more the active sites. This step depends not only on the porosity of the material but also on the availability of oxygenated species at the adsorbent surface and the formulation of EE2 which also contains only two OH functions. At pH 6.5 close to that of the majority of wastewater which does not exceed pH = 6 due to the dilution phenomenon, the EE2 hormone retains its OH character in its structure. Therefore, adsorption is governed by the interactions between the basic sites on the 40ZnHAP surface or even HAP with the EE2 molecules through the oxygenated groups on the surface of the adsorbent by hydrogen bonds. This hypothesis is supported by previous reports on the physisorption of phenol and its derivatives on hydroxyapatites [34, 36].

3.3 Photocatalytic Degradation of the Hormone

The direct photolysis of the hormone in water under UV light was carried out before any photocatalytic experiment in order to evaluate its contribution to the degradation of EE2 under only UV irradiation without a catalyst (Fig. 4). Results

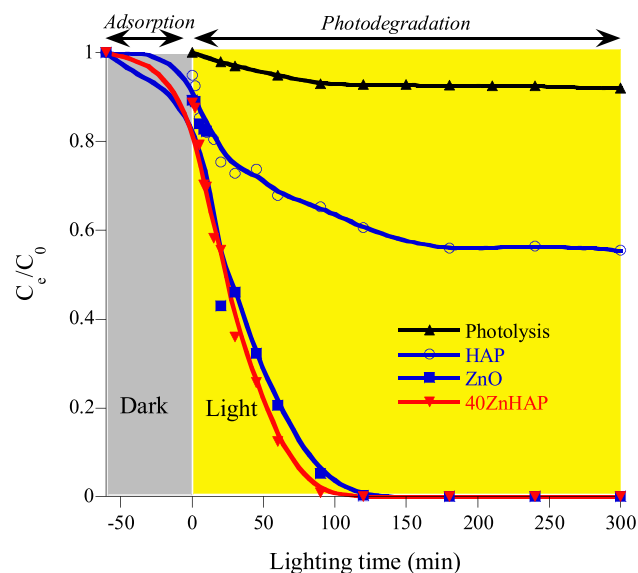


Fig. 4 Kinetics of photodegradation of 17α -ethinylestradiol hormone by the 40ZnHAP nanocomposite powder heated at 500°C compared to pure HAP and ZnO during a first 60 min period in the dark following by UV-irradiation

show no change in residual EE2 concentration with illuminating time indicating that any significant EE2 degradation without catalyst was observed. In the dark, all the catalysts show a slight decrease in the initial EE2 concentration, which was in good agreement with their previously obtained adsorption capacities. The small difference is explained by the variation in porosity between the three catalysts.

Using catalyst and under UV light, the degradation kinetics of the EE2 hormone supported on 40ZnHAP calcined at 500°C was studied and compared with those of HAP and ZnO under the same operating conditions. A complete EE2 degradation was observed using 40ZnHAP and ZnO photocatalysts at 90 min and 120 min as lighting time, respectively. The best catalytic efficiency is obtained on the 40ZnHAP catalyst, but very closed to that of ZnO. The advantage of the 40ZnHAP composite is related to the HAP porosity added to the ZnO semiconductor, which undoubtedly makes it possible to trap the photoproducts if they are form after catalytic degradation. However, the low photocatalytic efficiency of HAP is related to its high gap energy (5.3 eV) compared to those of 40ZnHAP (3.7 eV) and ZnO (3.2 eV) [35]. Eventually, 40ZnHAP catalyst showed the highest abilities to degrade the EE2 molecules. This suggests that the hydroxyapatite associated with ZnO improves the surface of the formed nanocomposite and activates the fixation of the EE2 and subsequently its photocatalytic efficiency. This approach is very interesting because the use of natural calcium and phosphate precursors from natural phosphate with a small ZnO amount reduces the manufacturing cost of 40ZnHAP as a photocatalytic agent for the

remediation of hormones and other pharmaceutical species. Its highly interconnected porous structure and the homogeneous dispersion of ZnO in the 40ZnHAP nanocomposite catalyst are favorable for instantaneous adsorption followed by effective photodegradation. Based on this observation, the nanocomposite catalyst can be an alternative to ZnO in several photocatalytic reactions.

The kinetics data were fitted with the linear form of the Langmuir–Hinshelwood equation: $\text{Ln} C_t/C_0 = -k_{\text{app}} t$, where C_0 and C_t are the initial and instantaneous EE2 concentrations (mg L^{-1}), respectively and k_{app} is the apparent pseudo-first-order rate constant (min^{-1}) determined from slope of the linear plot $\text{Ln} C_t/C_0$ against time t (Fig. 5). Based on the correlation coefficients (R^2), this model is most likely to characterize the degradation kinetics of the target molecules supported on the catalysts studied, indicating that the reaction follows the first order very well. For this first order kinetic, $t_{1/2}$ being a half-life time is calculated by the following relationship: $t_{1/2} = \text{Ln} 2/k_{\text{app}}$ providing a clear view of the persistence of this molecule in the environment. The rate constant k_{app} and $t_{1/2}$ are gathered in Table 4.

Results show that the rate constant and the time $t_{1/2}$ depend on the nature of the catalyst and it should be noted that the EE2 hormonal degradation kinetic over 40ZnHAP

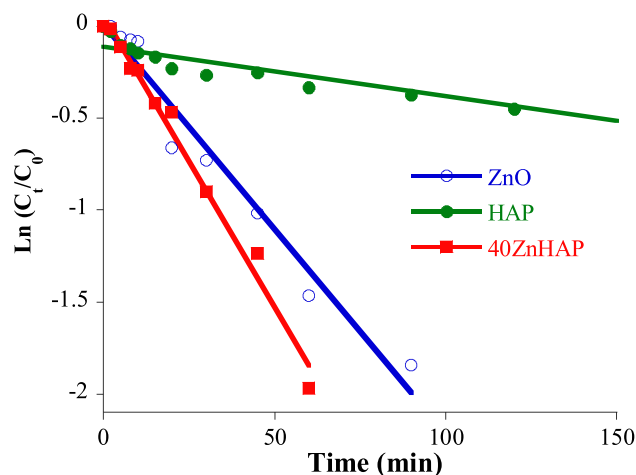


Fig. 5 Langmuir–Hinshelwood kinetic modeling curves of EE2 degradation by the synthesized nanocomposites compared to ZnO and HAP photocatalysts

Table 4 Kinetic constants and half-life of the EE2 hormone in the presence of different catalysts

	HAP	40ZnHAP	ZnO
k_{app} (min^{-1})	0.003	0.040	0.031
$t_{1/2}$ (min)	231.0	17.3	22.4
R^2	0.9309	0.9931	0.9840

nanocomposite was of the same order of magnitude and are similar to that of ZnO. Indeed, a synergy between the transfer of the hormone towards the catalyst surface and its porosity accelerates the kinetics of degradation under UV light which further favors the collisions of EE2 molecules with 40ZnHAP particles in decreasing the required activation energy.

According to our previous experimental results and those published elsewhere [24], it was found that photogenerated holes and superoxide radicals are the main active species responsible for the photocatalytic degradation of organic molecules on 40ZnHAP and ZnO photocatalysts. According to the results published elsewhere, the photocatalytic degradation of some antibiotics supported on the wZnHAP nanocomposites was very efficient and no HPLC peaks were detected related to the by-products at the end of the degradation reaction. [24]. As already proposed, this is explained by the adhesion of small amounts of fragmentation by the porous surface of the apatite, whereas the ZnO catalyst is a non-porous material. Therefore, advanced water treatment processes under UV light can generally achieve the complete removal of various toxic organic materials with the adsorption of by-products by the porous apatite surface. As detailed in our previous study [35], recycling of the 40ZnHAP catalyst was carried out to evaluate its stability and ensure the conservation of its photocatalytic efficiency

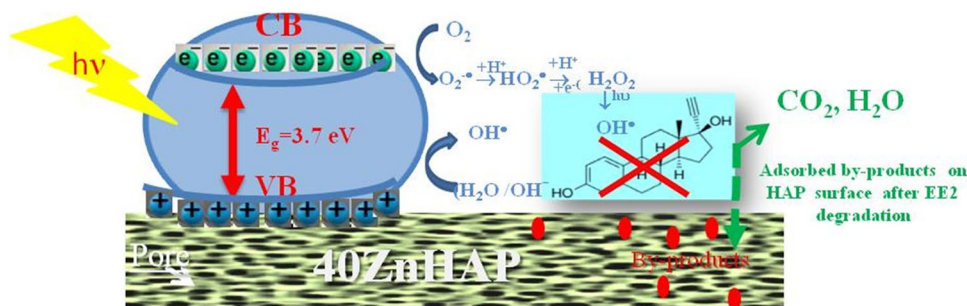
against degradation of the pharmaceutical pollutants after several cycles. After each photodegradation cycle the 40ZnHAP powder was washed with distilled water, and then dried in an oven overnight at 100 °C and heat treated at 500 °C for 3 h for the next degradation test. After four cycles, a 6% decrease in photocatalytic activity was recorded, and is linked to the loss of mass of the 40ZnHAP powder during washing, calcination, or even to the existence of by-products in the porous catalyst. The photocatalytic efficiency of 40ZnHAP was compared to other catalysts cited in the literature (Table 5). This nanocomposite is considered one of the most efficient photocatalysts, even for high hormonal concentrations, unlike other materials.

Under UV irradiation, the ZnHAP particles are at the origin of the energetic activation between the two bands CB \leftrightarrow VB, giving rise to very reactive species, which lead to the degradation of the hormone in the solution (Fig. 6). Moreover, $\bullet\text{OH}$ hydroxyl radicals cannot be produced directly by the photogenerated holes, but through the superoxides $\bullet\text{O}_2^-$ radicals which have a strong reducing power to react with H_2O or OH^- to obtain $\bullet\text{OH}$ [36, 45]. Based on the published studies and the discussions above, it is found that photogenerated holes and superoxide radicals are the main active species responsible for the photocatalytic degradation of the hormone on the 40ZnHAP photocatalyst. As has been demonstrated elsewhere on the degradation of

Table 5 Comparison of the photocatalytic efficiency of various catalysts towards EE2 degradation

Catalyst	Dose	[EE2] ₀	Source	Degradation (%)	Ref
Biodegradation	-	20 mg L ⁻¹	<i>R. palustris</i> strain	78 (long time)	[37]
UV/H ₂ O ₂	[H ₂ O ₂] ₀ = 5 mg L ⁻¹	2.63 mg L ⁻¹	UV (30W)	95% (100min)	[38]
TiO ₂ -doped zeolite	0.5 g L ⁻¹	10 mg L ⁻¹	UV	100% (40 min)	[39]
TiO ₂	0.5 g L ⁻¹	20 μg L ⁻¹	UVA (125 W)	85% (60 min)	[40]
CdS nano-rod/TiO ₂	0.5 g L ⁻¹	3 mg L ⁻¹	Visible	74.74% (120 min)	[41]
ZnO	1 g L ⁻¹	0.6 mg L ⁻¹	UVA	95% (60 min)	[42]
TiO ₂ (P25)	1.0 g L ⁻¹	0.6 mg L ⁻¹	UVA	100% (40 min)	
ZnO/Bi ₂ MoO ₆	-	5 mg L ⁻¹	Visible	74.74% (40min)	[43]
ZnO/TiO ₂	0.05 mg L ⁻¹	10 mg L ⁻¹	UV	95% (240 min)	[44]
C ₃ N ₄ /RGO/TiO ₂	0.5 g L ⁻¹	6 mg L ⁻¹	visible	100% (120min)	[45]
40ZnHAP	2 g L ⁻¹	10 mg L ⁻¹	UV (125 W)	100% (90min)	This study
ZnO	2 g L ⁻¹	10 mg L ⁻¹	UV (125 W)	100% (110)	

Fig. 6 Schematic diagram of the photodegradation mechanism of EE2 by porous 40ZnHAP nanocomposite showing the process of excitation and transfer of charge carriers in the nanocomposite



antibiotics supported on 40ZnHAP, no toxic species were found by bacteriological analysis carried out on an aqueous solution after photodegradation and subsequently the discharged water is healthy and that it does not contain toxic by-products, which is consistent with published HPLC analysis [24]. The absence of by-products in the final solution is explained either by a complete mineralization or by the trapping of these products by the porous apatite surface after such photodegradation of the pharmaceutical substances. In summary, the steps of the photocatalysis mechanism are as follows: (i) formation of charge carriers by absorption of photons; (ii) recombination of charge carriers; (iii) trapping an electron from the conduction band; (iv) trapping of a valence band hole at a porous 40ZnHAP surface; (v) initiation of an oxidative process.

4 Conclusions

The removal of 17 α -ethinylestradiol (EE2) from water as a hormonal model using an efficient 40ZnHAP nanocomposite was studied. The adsorption, photolysis and photocatalytic degradation of the hormone EE2 by the 40ZnHAP, ZnO and HAP catalysts were assessed using a multiple analysis approach. The main findings of the study are summarized as:

- The high ZnO content in 40ZnHAP nanocomposite induces efficient photocatalytic activity. This is related to the small size and better dispersion of ZnO in the HAP network, inducing a good porosity in the nanocomposite.
- Thanks to the gap energy of the 40ZnHAP nanocomposite close to that of ZnO, the electronic process occurs on the catalyst surface under UV photonic-radiation. The polluting particles are adsorbed on the catalyst surface and are then completely oxidized.
- The adsorption and photocatalytic degradation of EE2 by ZnO, HAP and 40ZnHAP nanocomposite follows the first-order kinetic model. The quantity of EE2 adsorbed is low on all the catalyst surfaces whereas a complete degradation was achieved using 40ZnHAP and ZnO at 90 min and 110 min, respectively.
- The association of ZnO with porous hydroxyapatite offers an innovative approach to improve photocatalytic performance for the degradation of organic contaminants, but also to capture the by-products formed after the end of the photocatalytic reaction.

Further studies on the photocatalytic oxidation of this and other hormones will be conducted under UV and natural sunlight conditions.

Funding None.

Declarations

Ethics Approval Not applicable.

Informed Consent Not applicable.

Conflict of Interest/Competing interests Not applicable.

References

1. Letsoalo MR, Sithole T, Mufamadi S, Mazhandu Z, Sillanpaa M, Kaushik A, Mashifana T (2023) Efficient detection and treatment of pharmaceutical contaminants to produce clean water for better health and environmental. *J Clean Prod* 387:135798
2. Papagiannaki D, Belay MH, Gonçalves NPF, Robotti E, Bianco-Prevot A, Binetti R, Calza P (2022) From monitoring to treatment, how to improve water quality: the pharmaceuticals case. *Chem Eng J Adv* 10:100245
3. Abbas KK, AbdulkadhimAl-Ghaban AMH, Rdewi EH (2022) Synthesis of a novel ZnO/TiO₂-nanorod MXene heterostructured nanophotocatalyst for the removal pharmaceutical ceftriaxone sodium from aqueous solution under simulated sunlight. *J Environ Chem Eng* 10:108111
4. Rashki O, Rezaei MR, Sayadi MH (2022) The high photocatalytic efficiency and stability of the Z-scheme CaTiO₃/WS₂ heterostructure for photocatalytic removal of 17 α -ethinyl estradiol in aqueous solution. *J Photochem Photobiol A: Chem* 43:114169
5. Bilal M, Rizwan K, Adeel M, Barceló D, Awad YA, Iqbal HMN (2022) Robust strategies to eliminate endocrine disruptive estrogens in water resources. *Envir Poll* 306:119373
6. Bouyarmane H, El Hanbali I, El Karbane M, Rami A, Saoiabi A, Saoiabi S, Masse S, Coradin T, Laghzizil A (2015) Parameters influencing ciprofloxacin, ofloxacin, amoxicillin and sulfamethoxazole retention by natural and converted calcium phosphates. *J Hazard Mater* 291:38–44
7. Sang D, Cimetiere N, Giraudet S, Tan R, Wolbert D, Le Cloirec P (2022) Adsorption-desorption of organic micropollutants by powdered activated carbon and coagulant in drinking water treatment. *J Water Process Eng* 49:103190
8. Zhai C, Chen Y, Huang X, Isaev AB, Zhu M (2022) Recent progress on single-atom catalysts in advanced oxidation processes for water treatment. *Environ Functional Matre* 1:2019–2229
9. García-Araya JF, Beltrán FJ, Aguinaco A (2010) Diclofenac removal from water by ozone and photolytic TiO₂ catalysed processes. *J Chem Technol Biotechnol* 85:798–804
10. Elmolla ES, Chaudhuri M (2010) Comparison of different advanced oxidation processes for treatment of antibiotic aqueous solution. *Desalination* 256:43–47
11. Al-Hajji LA, Ismail AA, Bumajdad A, Alsaidi M, Ahmed SA, Al-Hazza A, Ahmed N (2021) Photodegradation of powerful five estrogens collected from waste water treatment plant over visible-light-driven Au/TiO₂ photocatalyst. *Environ Technol Innov* 24:101958
12. Munguti LK, Dejene FB, Muthee DK (2023) High photodegradation performance of ZnO nanoparticles supported on porous Zeolite Na-A: effects of ZnO loading. *Mater Chem Phys* 295:127063
13. Mao K, Li Y, Zhang H, Zhang W, Yan W (2013) Photocatalytic Degradation of 17 α -ethinylestradiol and inactivation of escherichia coli using Ag-Modified TiO₂ nanotube arrays. *Clean-Soil Air Water* 41:455462
14. Islam SU, Bairagi S, Kamali MR (2023) Review on green biomass-synthesized metallic nanoparticles and composites and

- their photocatalytic water purification applications: progress and perspectives. *Chem Eng J Adv* 14:100460
15. Arevalo-Perez JC, Cruz-Romero D, Cordero-García A, Lobato-García CE, Aguilar-Elguezabal A, Torres-Torres JG (2020) Photodegradation of 17 α -methyltestosterone using TiO_2 - Gd^{3+} and TiO_2 - Sm^{3+} , Photocatalysts and simulated solar radiation as an activation source. *Chemosphere* 249:126497
 16. Nguyen THA, Doan VD, Tran AV, Nguyen VC, Vasseghian Y (2021) Green synthesis of Nb-doped ZnO nanocomposite for photocatalytic degradation of tetracycline antibiotic under visible light. *Mater Lett* 308:131129
 17. Yashni G, Al-Gheethi A, Mohamed R, Hossain MS, Kamil AF, Shanmugan VA (2021) Photocatalysis of xenobiotic organic compounds in greywater using zinc oxide nanoparticles: a critical review. *Water Environ J* 35:190–217
 18. Bettini S, Pagano R, Valli D, Ingrosso C, Roeffaers M, Hofkens J, Giancane G, Valli L (2023) ZnO nanostructures based piezo-photocatalytic degradation enhancement of steroid hormones. *Surf Interfaces* 36:102581
 19. Elsayed MS, Ahmed IA, Bader DMD, Hassan AF (2022) Green synthesis of nano zinc oxide/nanohydroxyapatite composites using date palm pits extract and eggshells: adsorption and photocatalytic degradation of methylene blue. *Nanomaterials* 12:49
 20. Fatta-Kassinos D, Vasquez MI, Kümmerer K (2011) Transformation products of pharmaceuticals in surface waters and wastewater formed during photolysis and advanced oxidation processes-Degradation, elucidation of byproducts and assessment of their biological potency. *Chemosphere* 85:693–709
 21. Shabbir S, Faheem M, Dar AA, Ali N, Kerr PG, Yu ZG, Li Y, Frei S, Albasher G, Gilfedder BS (2022) Enhanced periphyton biodegradation of endocrine disrupting hormones and microplastic: Intrinsic reaction mechanism, influential humic acid and microbial community structure elucidation. *Chemosphere* 293:133515
 22. Go AD, dela Rosa FM, Camacho DH, Punzalan ER (2022) Dataset on photocatalytic degradation of Levofloxacin using hydroxyapatite photocatalyst: optimization by response surface methodology. *Data Brief* 42:108219
 23. Bouyarmane H, El Bekkali C, Labrag J, Es-Saidi I, Bouhnik O, Abdelmoumen H, Laghzizil A, Nunzi JM, Robert D (2021) Photocatalytic degradation of emerging antibiotic pollutants in waters by TiO_2 /Hydroxyapatite nanocomposite materials. *Surf Interfaces* 24:101155
 24. El Bekkali C, Bouyarmane H, El Karbane M, Masse S, Saoiabi A, Coradin T, Laghzizil A (2018) Zinc oxide-hydroxyapatite nanocomposite photocatalysts for the degradation of ciprofloxacin and ofloxacin antibiotics. *Colloids Surf A* 539:364–370
 25. Go AD, dela Rosa FM, Camacho DH, Punzalan ER (2024) Photocatalytic degradation of levofloxacin using ZnO/hydroxyapatite nanocomposite: optimization using response surface methodology. *Chem Data Coll* 50:101126
 26. He C, Yin Z, He J, Lv J, Wang C (2022) Occurrence and photodegradation of typical steroid hormones in surface water of urban lakes in Wuhan, China. *J Environ Chem Eng* 10:108602
 27. Martins de Barros R, Lissalde S, Guibal R, Guibaud G (2022) Development of a multi-hormone analysis method by LC-MS/MS for environmental water application using diffusive gradient in thin films. *Talanta* 243:12339
 28. Ribeiro TSS, Mourão LC, Souza GBM, Dias IM, Andrade LA, Souza PLM, Cardozo-Filho L, Oliveira GR, Oliveira SB, Alonso CG (2021) Treatment of hormones in wastewater from the pharmaceutical industry by continuous flow supercritical water technology. *J Environ Chem Eng* 9:106095
 29. Wang L, Cui X, Xu J, Wang G, Guo M, Yu L, Yang K, Luo Z, Zeng A, Chen G, Zhang J, Fu Q (2022) Highly efficient amino-functionalized aluminum-based metal organic frameworks mesoporous nanorods for selective extraction of hydrocortisone in pharmaceutical wastewater. *J Pharm Biomed Anal* 219:11493
 30. Escudeiro de Oliveira M, Barroso BL, De Almeida J, Moraes MLL, Rodrigues CA (2020) Photoelectrocatalytic degradation of 17 α -ethinylestradiol and estrone under UV and visible light using nanotubular oxide arrays grown on Ti-0.5wt%W. *Environ Res* 191:110044
 31. El Asri S, Laghzizil A, Saoiabi A, Alaoui A, El Abbassi K, M'Hamdi R, Coradin T (2009) A novel process for the fabrication of nanoporous apatites from Moroccan phosphate rock. *Colloids Surf A* 35:73–78
 32. Joint Committee on Powder Diffraction Standards (JCPDS) (2003) Powder diffraction files; international Centre for diffraction data (ICDD): Newton Square, PA, USA
 33. Hazrah KS, Antao SM (2022) Apatite, $\text{Ca}_{10}(\text{PO}_4)_6(\text{OH}, \text{F}, \text{Cl})_2$: structural variations natural solid solutions, intergrowths, and zoning. *Minerals* 12:527
 34. Bahdod A, El Asri S, Saoiabi A, Coradin T, Laghzizil A (2009) Adsorption of phenol from an aqueous solution by selected apatite adsorbents: kinetic process and impact of the surface properties. *Water Res* 43:313–318
 35. El Bekkali C, Labrag J, Oulguidoum A, Chamkhi I, Laghzizil A, Nunzi JM, Robert D, Aurag J (2022) Porous ZnO/hydroxyapatite nanomaterials with effective photocatalytic and antibacterial activities for the degradation of antibiotics. *Nanotechnol Environ Eng* 7:1
 36. Lin K, Pan J, Chen Y, Cheng R, Xu X (2009) Study the adsorption of phenol from aqueous solution on hydroxyapatite nanopowders. *J Hazard Mater* 161:231–240
 37. Syed Z, Sogani M, Kumar A, Rajvanshi J, Sharma G, Sonu K (2022) Biodegradation of synthetic estrogen using bioelectrochemical system and degradation pathway analysis through Quadrupole-time-of-flight-mass spectrometry. *Biores Technol* 349:126857
 38. Feng Y, Ren N (2010) Kinetic degradation model and estrogenicity changes of EE2 (17 α -ethinylestradiol) in aqueous solution by UV and UV/ H_2O_2 technology. *J Hazard Mater* 181:1127–1133
 39. Pan Z, Stemmler EA, Cho HJ, Fan W, LeBlanc LA, Patterson HH, Amirbahman A (2014) Photocatalytic degradation of 17-ethinylestradiol (EE2) in the presence of TiO_2 -doped zeolite. *J Hazard Mater* 279:17–25
 40. Schneider JT, Nagata N, Peralta-Zamora P (2018) Suspended and immobilized TiO_2 photocatalytic degradation of Estrogens: Potential for application in wastewater treatment processes. *J Braz Chem Soc* 29:380–389
 41. Luo L, Longa J, Zhao S, Dai J, Ma L, Wang H, Xiaa L, Shu L, Jiang F (2019) Effective visible-light-driven photocatalytic degradation of 17-ethinylestradiol by crosslinked CdS nanorod/ TiO_2 (B) nano-belt composite. *Process Saf Environ Prot* 130:77–85
 42. Han J, Liu Y, Singhal N, Wang L, Gao W (2012) Comparative photocatalytic degradation of estrone in water by ZnO and TiO_2 under artificial UVA and solar irradiation. *Chem Eng J* 213:150–162
 43. Shi X, Wu S, Yang C, Li L, Li H, Jiang F, Luo L (2023) Understanding the synergistic adsorption-photocatalytic degradation of EE2 using ZnO/ Bi_2MoO_6 (010). *J Alloys Compd* 968:172118
 44. Menon NG, George L, Tatiparti SS, Mukherji S (2021) Efficacy and reusability of mixed-phase TiO_2 -ZnO nanocomposites for the removal of estrogenic effects of 17 β -Estradiol and 17 α -Ethinylestradiol from water. *J Environ Manag* 288:112340

45. Luo L, Meng D, He L, Wang X, Xia L, Pan X, Jiang F, Wang H, Dai J (2022) Photocatalytic activation of peroxydisulfate by a new porous g-C₃N₄/reduced graphene oxide/TiO₂ nanobelts composite for efficient degradation of 17 α -ethinylestradiol. *Chem Eng J* 446:137325

Springer Nature or its licensor (e.g. a society or other partner) holds exclusive rights to this article under a publishing agreement with the author(s) or other rightsholder(s); author self-archiving of the accepted manuscript version of this article is solely governed by the terms of such publishing agreement and applicable law.